TFPT Prediction: Achromatic Residual Polarization Intercept around Compact Objects

An EHT/ngEHT Test of the Local Dyonic β_{BH} Channel

Stefan Hamann Alessandro Rizzo

Standalone prediction note – April 27, 2026

Abstract

This note isolates a new TFPT observation channel: a structured, achromatic residual intercept of the linear-polarization angle in the magnetised inflow region of a horizon-scale black hole. The residual is sectorised away from the cosmological birefringence row of the determinant-line response. Its amplitude is fixed by the same admissibility/index data that controls the fine-structure constant and the cosmic-birefringence seed; only the geometric and emission factors carrying the local effective $E\cdot B$ structure are model dependent.

Prediction scope and audit

Target. $\beta_{\mathrm{BH}}(r) \sim \dfrac{Q_e^{\mathrm{eff}}\, Q_m^{\mathrm{eff}}}{256\pi^4\, r^2}$, achromatic and structured.
Status. Physical observable; local dyonic projection of the determinant-line response. Coupling fixed; geometric weights model dependent.
Dependency class. determinant response R_{CS}, dyonic projection on the horizon collar.
Kill or pressure test. calibrated achromatic residual intercept χ_0^{res} statistically consistent with zero across the horizon-scale image at the declared sensitivity.

1 Standalone Minimal Kernel

Minimal TFPT kernel used in this prediction

The standalone input package is the boundary-polarized closed branch

$$\mathfrak{S}_{\mathrm{min}} \Rightarrow \mathcal{B}_{\mathrm{min}} \Rightarrow \mathfrak{T}_{\partial}^{\mathrm{min}} \Rightarrow (\tau_{\mathrm{dbl}}, \iota_C, P_{\mathrm{prim}}, [u_\Sigma], c_3) \Rightarrow d^{\star}_{\mathrm{disc}} \Rightarrow P_{\mathrm{adm}} \Rightarrow \mathfrak{T}_{\star}.$$

The prediction uses only the sector map named in its audit box. Numerical comparison conventions are not theorem inputs; they enter only at the final interface row.

This row uses the same closed-branch input package as the cosmic-birefringence prediction. The new content is the projection map onto the local dyonic geometry of a magnetised compact object. Source status follows the TFPT 4.5 split: boundary, carrier, and electromagnetic-closure inputs are core; the determinant-line response is a bridge readout; cosmology and astrophysical projections are downstream comparison surfaces.

2 Dependency Graph

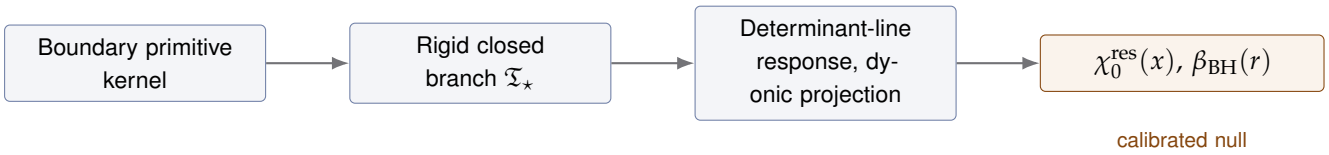

Local $E\cdot B$ projection on the horizon collar after GRMHD subtraction.

3 From the Determinant-Line Response to a Local Channel

The determinant-line response of TFPT yields the cosmological birefringence row through

$$\beta_{\rm rad} = \frac{\varphi_0^{\rm ret}}{4\pi}, \qquad \beta = \beta_{\rm rad} \times \left(\frac{180^\circ}{\pi}\right) \approx 0.2424^\circ.$$

The same admissibility data emits a *local* astrophysical β amplitude for a magnetised horizon-scale region. Tracing the dyonic appendix of the TFPT 4.2 source through the closure chain $\mathfrak{T}_\star \to R_{\rm CS} \to$ local response, the local rotation rate takes the structured form

$$\beta_{\rm BH}(r) \;=\; \frac{Q_e^{\rm eff}(x)\,Q_m^{\rm eff}(x)}{256\pi^4\,r^2} \;=\; 16\,c_3^4\,\frac{Q_e^{\rm eff}(x)\,Q_m^{\rm eff}(x)}{r^2} \;=\; \frac{\delta_{\rm top}}{3}\,\frac{Q_e^{\rm eff}(x)\,Q_m^{\rm eff}(x)}{r^2}, \tag{1}$$

where $c_3 = \frac{1}{8\pi}$ is the fixed coupling normaliser of Paper 1 and $\delta_{\rm top} = 48c_3^4$ is the same topological coefficient that fixes the α-kernel correction in Paper 3. The product $Q_e^{\rm eff}\,Q_m^{\rm eff}$ encodes the local effective $E\cdot B$ structure on the horizon collar and is treated below as a model-dependent geometric weight.

Remark (Coupling fixed, geometry model dependent). The numerical coefficient $1/(256\pi^4) = 16c_3^4$ is fixed by the same TFPT branch data that controls α and $\beta_{\rm rad}$ — there is no free coupling here. What is *not* fixed by TFPT alone is the spatial profile of the effective dyonic charges $Q_e^{\rm eff}(x)$, $Q_m^{\rm eff}(x)$, the inflow geometry, and the emission radius; these are MHD/GR inputs of the source model. The TFPT claim is therefore the structured shape and sign pattern of the residual, not a parameter-free amplitude prediction at one pixel of the image.

4 Observation Protocol

The conventional rotation-measure decomposition of the linear-polarization angle is

$$\chi(x,\lambda^2) \;=\; \chi_0(x) + {\rm RM}(x)\,\lambda^2 + \epsilon, \tag{2}$$

i.e. the wavelength-squared coefficient ${\rm RM}(x)$ captures conventional Faraday rotation and the intercept $\chi_0(x)$ collects the achromatic part: intrinsic emission orientation, calibration, and any new physics insensitive to λ^2.

The TFPT contribution sits inside $\chi_0(x)$. To isolate it we work with the achromatic *residual intercept*

$$\chi_0^{\rm res}(x) \;=\; \chi_0^{\rm obs}(x) \;-\; \chi_0^{\rm GRMHD}(x), \tag{3}$$

where $\chi_0^{\rm GRMHD}(x)$ is the achromatic intercept produced by the calibrated intrinsic-emission and astrophysical-modelling pipeline of the chosen GRMHD/synchrotron forward model. The TFPT prediction is then a structured pattern in $\chi_0^{\rm res}(x)$, not a generic "intercept different from zero".

Achromatic residual-intercept test

Step 1 — Multi-frequency map. Build a per-pixel polarization-angle map $\chi(x,\lambda^2)$ across at least three frequency bands. Fit (2) per pixel.

Step 2 — Forward subtraction. Subtract the GRMHD/synchrotron pipeline's prediction for the achromatic intercept $\chi_0^{\mathrm{GRMHD}}(x)$, including calibration and intrinsic emission orientation, to obtain the residual map $\chi_0^{\mathrm{res}}(x)$.
Step 3 — Spatial pattern. Test the residual map for the structured $1/r^2$ amplitude profile (1) along the bright magnetically dominated lensed regions of the horizon-scale image, accumulated against the local effective-$E\cdot B$ orientation.
Step 4 — Sign-flip null. Confirm or reject the TFPT-predicted sign flip of χ_0^{res} when the effective $E\cdot B$ orientation reverses (e.g. when one compares two regions of opposite jet-orientation context, or jet vs. counter-jet sectors).
Step 5 — Frequency null. Confirm that the surviving structured component is achromatic: no detectable λ^2 dependence beyond the fitted $\mathrm{RM}(x)$ term.

5 Three Independent Nulls

The prediction is robust because three independent null tests must be passed simultaneously before it can be claimed:

1. **Frequency-null.** The TFPT residual must be *achromatic*: any structured component remaining after (2) that scales with λ^2 does not belong to this channel.
2. **Spatial-null.** The TFPT residual is required to follow the structured $1/r^2$ profile of (1); a spatially uniform residual is calibration, not the determinant-line projection.
3. **Sign-flip null.** The TFPT residual must reverse sign when the effective $E\cdot B$ orientation reverses; a residual that does not flip is also calibration.

6 Cross-Link to the α-Kernel

The local dyonic amplitude in (1) carries the same topological coefficient that controls the precision-zone correction of the α-kernel:

$$\delta_{\mathrm{top}} \;=\; 48\,c_3^4, \qquad \beta_{\mathrm{BH}}(r) \;=\; \frac{\delta_{\mathrm{top}}}{3}\,\frac{Q_e^{\mathrm{eff}}\,Q_m^{\mathrm{eff}}}{r^2}.$$

This cross-link is structural, not numerical: the same TFPT branch number that puts the electromagnetic closure into the precision zone of CODATA also controls the size of the local dyonic intercept. EHT-class polarimetry therefore probes the same admissibility data as the α row, only projected onto the local horizon collar instead of the asymptotic Thomson limit.

7 No-Knobs and Failure Surface

No-knobs audit

The TFPT coupling $1/(256\pi^4) = 16c_3^4$ is fixed by the same kernel that fixes α and β_{rad}: there is *no free coupling* in (1). The model-dependent ingredients are the geometric weights $Q_e^{\mathrm{eff}}(x)$ and $Q_m^{\mathrm{eff}}(x)$, the inflow geometry, and the emission radius. A structured, achromatic residual $\chi_0^{\mathrm{res}}(x)$ statistically consistent with zero across the horizon-scale image, after honest GRMHD subtraction, and at the declared sensitivity, falsifies this row. A residual without the predicted spatial $1/r^2$ shape, without sign reversal under effective $E\cdot B$ flips, or with measurable λ^2 dependence, also falsifies it.

8 Minimal Submission Claim

The standalone claim is limited to the structured achromatic residual intercept, its sign-flip behaviour, and its $1/r^2$ profile in the magnetised horizon collar. It does *not* claim a full microscopic black-hole solution and does *not* reinterpret rotation-measure analyses. Any update of the upstream boundary kernel, carrier theorem, electromagnetic closure, or determinant-line response must be propagated into this prediction before the protocol is distributed.

References

[1] M. F. Atiyah, V. K. Patodi, and I. M. Singer, *Spectral asymmetry and Riemannian geometry. I*, Math. Proc. Cambridge Philos. Soc. **77** (1975), 43–69.

[2] A. H. Chamseddine and A. Connes, *The spectral action principle*, Commun. Math. Phys. **186** (1997), 731–750.

[3] P. J. Mohr, D. B. Newell, and B. N. Taylor, *CODATA recommended values of the fundamental physical constants: 2022 update*, NIST / CODATA reference set, accessed March 2026.

[4] S. Navas et al. (Particle Data Group), *Review of Particle Physics*, Phys. Rev. D **110** (2024), 030001; 2025 online update.

[5] NuFIT Collaboration, *NuFIT global analysis of neutrino oscillation data*, website snapshot based on data available through November 2025.

[6] Planck Collaboration, *Planck 2018 results. VI. Cosmological parameters*, Astron. Astrophys. **641** (2020), A6.

[7] Y. Minami and E. Komatsu, *New extraction of the cosmic birefringence from the Planck 2018 polarization data*, Phys. Rev. Lett. **125** (2020), 221301.

[8] X. Chang et al. (for the NA62 Collaboration), *New measurement of $K^+ \to \pi^+ \nu\bar{\nu}$ branching ratio at the NA62 experiment*, arXiv:2604.12649.

[9] KOTO Collaboration, *Search for the $K_L \to \pi^0 \nu\bar{\nu}$ decay at the J-PARC KOTO experiment*, arXiv:2411.11237.